Proceedings of the ASME 2010 3rd Joint US-European Fluids Engineering Summer Meeting and
8th International Conference on Nanochannels, Microchannels, and Minichannels
FEDSM-ICNMM2010
August 1-5, 2010, Montreal, Canada

FEDSM-ICNMM2010-30772

NUMERICAL ANALYSIS OF THE EFFECT OF DIFFERENT CHANNEL GEOMETRIES AND ELECTRODE MATERIALS ON THE PERFORMANCE OF MICROFLUIDIC FUEL CELLS

Ali Ebrahimi Khabbazi
University of British Columbia
Kelowna, BC, Canada
ali.ebrahimi@ubc.ca

Andrew Richards
University of British Columbia
Kelowna, BC, Canada
richaj@interchange.ubc.ca

Mina Hoorfar
University of British Columbia
Kelowna, BC, Canada
mina.hoorfar@ubc.ca

ABSTRACT

A typical microfluidic fuel cell is comprised of a Y- or T-shaped microchannel. The fuel and the oxidant streams are introduced from the two different inlets. The anodic and cathodic flows meet each other at the beginning of the main channel and start to travel together along the channel. Due to the fact that the viscous forces dominate the inertia forces in microchannels, the oxidant and the fuel streams establish a side-by-side co-laminar flow which makes the anolyte and catholyte flow together without turbulent mixing. Laminar flow in microfluidic fuel cells plays the role of the membrane in proton exchange membrane (PEM) fuel cells by maintaining the separation of the fuel and oxidant. This eliminates the need for the membrane and overcomes the membrane-related issues such as the ohmic overpotential and water management which are relevant to PEM fuel cells. In addition to the above advantage, the high surface-to-volume ratio of these micron-scale devices contributes to their high power density. This advantage is due to the fact that the electrochemical reactions in fuel cells are surface-based. The electrodes on which the electrochemical reactions are occurring are installed appropriately on the walls of the channel in a way that reacting flows are restricted to the proper electrodes. Since the flow is laminar the performance of the microfluidic fuel cell significantly depends on the device geometry. In this paper, different channel geometries and different electrode configurations are modeled and their performances are compared through the polarization curves. It has been found that the high aspect ratio provides the largest power density. In this work, the performance of the flow-through porous electrode was also modeled and compared against the conventional non-porous electrode microfluidic fuel cells. The flow-through porous electrode design is based on cross-flow of aqueous vanadium redox species through the electrodes into an exit channel, where the waste solutions meet and establish a co-laminar flow. This co-laminar flow of reacted species facilitates ionic charge transfer in a membraneless configuration. It has been found that the flow-through porous architecture provides an increased active surface area which contributes to a higher power density as opposed to the fuel cells with non-porous electrodes.

INTRODUCTION

Recently, there has been a growing demand for small but high power sources of energy for portable devices which are expected to function for long periods of time without the need for recharging [1] (such as global positioning systems, laptops and mobile phones). The current battery technology can hardly keep up with this growing power demand [2]. A recent comparison between Li-ion batteries and fuel cells has shown that the latter has much higher power density, and hence more potential to respond to the future market) [2]. Since the reactions in fuel cells are surface based, miniaturization of fuel cells, which increases the surface-to-volume ratio, leads to even further improvements in the power density that is required for portable devices [3, 4]. Thus, miniaturized fuel cells are capable of bridging the gap between the battery technology and the high power density required for the portable applications. A prodigious amount of research has been conducted on the miniaturization of the conventional fuel cells [5-7]. Although the energy density of the miniaturized fuel cells increases as their size continues to shrink, several technological and mechanical challenges (e.g., efficiency issues related to water and heat management, the ohmic overpotential caused by the membrane, and machining of the graphite bipolar plates) still remain [6, 8]. These challenges limit the further decrease in the size, and hence limit the increase in the power density of the miniaturized fuel cells.

Recently, a novel design and structure of the fuel cell, called the microfluidic fuel cell, has been introduced to overcome the above limitations of miniaturized fuel cells. Figure 1 presents the schematic of a typical Y-shaped microfluidic fuel cell. In such systems, the fuel and oxidant are introduced into a microchannel through separate inlets and form a side-by-side co-laminar flow between the electrodes, which are typically positioned along the channel. Laminar flow maintains separation of the fuel and oxidant. This eliminates the need for the membrane and overcomes the membrane-related issues (such as the ohmic overpotentials and water management) mentioned for the miniaturized fuel cells. Due to the laminar nature of the flow in these systems, the transport phenomenon is diffusion limited, and hence the channel geometry plays an important role. As the fuel and oxidant streams travel down the channel the inter-diffusion region (i.e., mixing region) is established and grows due to the transportation of reactants from their own side to the other side through diffusion. This mixing region limits the amount of the reactants that can be potentially available to the electrodes. At the same time, there is a concentration boundary layer forming on each electrode as the fluid is traveling toward the end of the channel. This concentration boundary layer (also known as depletion layer) is acting as a resistance for the reactants to reach to the active surfaces; therefore, it is desirable to have a thin depletion layer all over the electrodes.

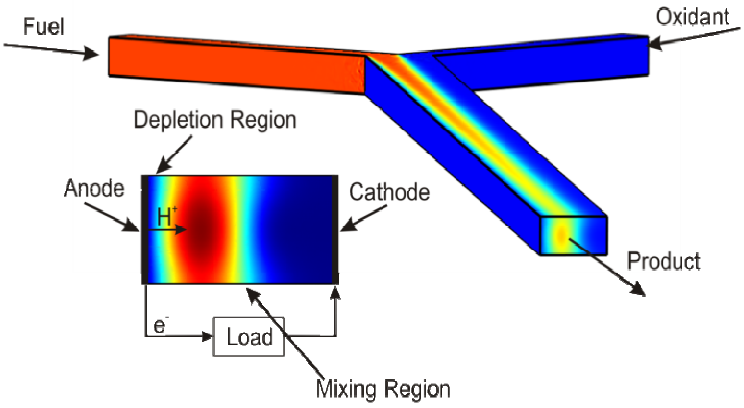

Figure 1 A schematic of a typical microfluidic fuel cell

Bazylak et al. [1] tested three different channel cross sections with different aspect ratios, obtained the fuel and oxidant distribution, and calculated the fuel utilization. They found that the rectangular cross sections have higher fuel utilization compared to the square ones. Chang et al. [9] also conducted a numerical analysis for a fixed flow rate and a fixed channel cross section aspect ratio (i.e., height to width ratio). They reported that the reduction of cross-sectional area results in higher fuel cell performance. They also observed that for a constant cross sectional area, the high aspect ratio results in a higher cell performance. The improved performance can be associated with two facts: 1) the higher the channel height, the higher the Peclet number (i.e., $Pe = UH/D$ which represents the convective to diffusive transport.). The higher the Peclet number the faster the depletion regions are filled with fresh reactants, so higher current is produced by the cell; 2) in high aspect ratio geometries, the anode and cathode electrodes are closer to each other; therefore, the proton resistivity of the electrolyte presented in the following equation is reduced :[10]

$$R_f = \frac{d}{\sigma A} \qquad (1)$$

In this equation, R_f is the ohmic resistance for ionic transport, d represents the distance between the anode and cathode, σ refers to ionic conductivity and A is the cross-sectional area of the charge transfer.

In the microfluidic fuel cell, there is always a trade-off between the power density and the overall energy conversion efficiency, which is directly proportional to fuel utilization. Microfluidic fuel cells with porous electrodes (see Fig. 2) are introduced by Kjeang et al. [11] to overcome this issue. In this design, the reactants are forced to pass through the porous electrodes, which are porous carbon strips. The waste solutions from the anode side and cathode side come to meet each other in the central channel in which they establish a side-by-side co-laminar flow traveling toward the end of the channel. This electrolyte solution is responsible for the ionic charge transfer between the anode and cathode. The porous-structured design improves fuel utilization by increasing the active surface area without significant parasitic pumping load [12].

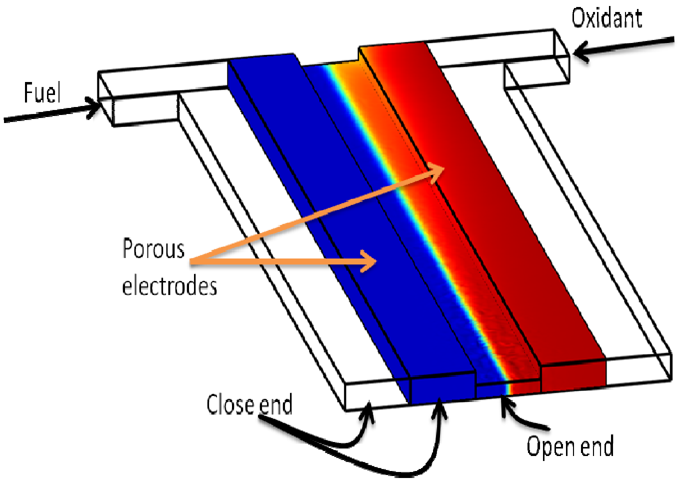

Figure 2 A schematic of a microfluidic fuel cell with flow-through porous electrodes

The most common anolyte/catholyte streams in the porous-structured design are vanadium redox couples as they do not require expensive catalysts such as Pt for electrochemical reactions (the reactions take place on the bare carbon electrodes). The electrochemical reactions for such streams are:

$$V^{3+} + e^- \Leftrightarrow V^{2+} \qquad (2)$$

$$VO_2^{\ +} + 2H^+ + e^- \Leftrightarrow VO^{2+} + H_2O$$

However, the microfluidic fuel cell with solid electrode uses formic acid as the fuel and an aqueous solution of sulfuric acid saturated with oxygen as the oxidant. Although hydrogen is one of the best fuels for the PEM fuel cells, the safety concerns due to the high-pressure storage tank, especially in microscale devices, prevent its usage in the microfluidic fuel cell [16]. Beside the above-mentioned fact, it is to some extent hard for two gaseous streams to establish a side-by-side co-laminar flow with a thin mixing region in between. Also, the gaseous species have higher diffusion coefficient compared to the aqueous solutions. This leads to a very wide inter-diffusion region which particularly limits the amount of the electrode surface area that could be installed. Most of the studies [17, 18] on the microfluidic fuel cells have also focused on the devices using liquid fuels due to their convenient storage. Methanol and formic acid are two examples of aqueous fuels which are typically used in microfluidic fuel cells due to their higher energy density compared to the gaseous ones. In this paper, formic acid has been selected as the fuel, for the microfluidic fuel cell with solid electrodes, as it has been reported to be electrochemically more active compared to methanol [1]. The oxidation of formic acid and reduction of oxygen in the microfluidic fuel cells presented as

$$HCOOH \rightarrow CO_2 + 2H^+ + 2e^- \qquad (3)$$

$$O_2 + 4H^+ + 4e^- \rightarrow 2H_2O$$

Modeling of the different types of microfluidic fuel cells which are mentioned above requires extensive and difficult experimental studies which are conducted to design and obtain high performance and efficient microfluidic fuel cells. The effort to design an innovative cell can be significantly reduced by developing an accurate numerical model monitoring the cell performance as modifications are added to the original designs. The development of an accurate model capturing the phenomena occurring in this system, however, is not a trivial task. This paper presents, 3–D numerical simulation developed using the COMSOL Multiphysics toolbox to determine the performance of different microfluidic fuel cell designs. To verify the accuracy of the simulation, first it was used to develop a model for a 30 mm long channel for which the formulations are similar to those reported by Chang et al. [9]. The two models were compared. Figure 3 shows this comparison. It is clear that the results of the presented model in this paper are in agreement with those reported before [9]. However, the time required to run the simulation is long (approximately 10 hours). Therefore, an 8 mm long channel is used in this study to make the modeling time efficient without influencing the ultimate objective which is to study the effect of different aspect ratio structures and materials have on the final power output of the microfluidic fuel cell. The porous design is a numerical reproduce of the experiment performed by Kjeang et.al. [11].

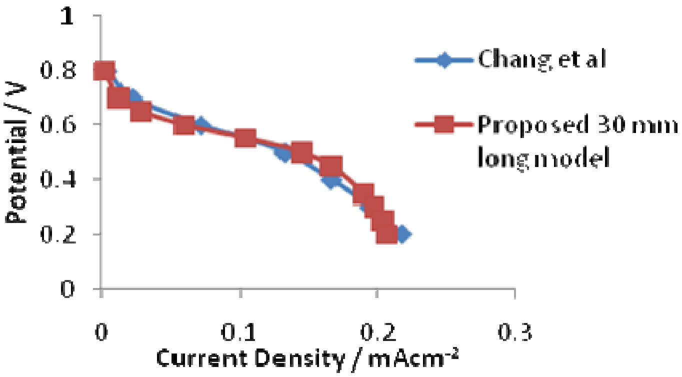

Figure 3 Verification of the proposed model against the results reported by Chang et al. [9]

NOMENCLATURE

C	Concentration
D	Diffusion coefficient
N	Number of electrons transferred
T	Cell temperature
I_0	Exchange current density
A	Charge transfer coefficient
ε_0	Reference value for porosity
Σ	Ionic conductivity
V	Velocity
P	Fluid density
P	Pressure
M	Viscosity
S	Reactant consumption rate
A_e	Reference value of specific surface area
φ	Local potential

GEOMETERY

This section presents the microfluidic fuel cell geometries considered for the numerical analysis. The basic geometry is comprised of a Y-shaped channel with 1mm×1mm main cross section and 0.5mm×1mm inlet cross sections. Figure 4 depicts the different channel cross section aspect ratios and electrode configurations.

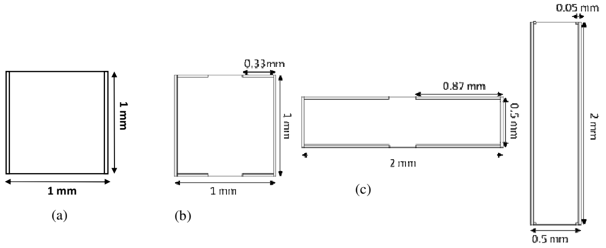

Figure 4 The schematics and dimensions of different cross–section aspect ratios and electrode geometries are presented in (a), (b), (c), and (d) which are referred to a the "Simple square", "Extended square", "Low aspect ratio" and "High aspect ratio", respectively.

MODELING

In order to predict the effect of activation, ohmic, and concentration overpotentials on fuel cell performance, a set of steady-state conservation equations is used to model fuel cell operation. The values of the various parameters used in the model are given in the Annex A and B.

Microfluidic flows are characterized by low Reynolds numbers due to the small dimensions of microchannels and low fluid velocities. Applying mass and momentum conservation in differential form allows the velocity field to be described by the Navier-Stokes and continuity equations [19].

$$\nabla \cdot \mathrm{v} = 0 \tag{4}$$

$$\rho(\mathrm{v} \cdot \nabla \mathrm{v}) = -\nabla p + \mu \nabla^2 \mathrm{v}$$

The permeability of the porous electrodes is defined by the Carman-Kozeny equation, which is one of the most commonly-used models for description of porous media permeation in the literature [11 from porous paper]. This equation is given as

$$K = \frac{d_f^2 \varepsilon^3}{16 k_{CK} (1-\varepsilon)^2} \tag{5}$$

In these equations, v and p are the velocity and pressure, respectively. ρ and μ represent the density and viscosity which both are assumed to be equal for the two streams and constant over the whole domain.

The transport of charged species and the electric field within the electrolyte can be modeled using the potential equation. The equation describing the electric field within the electrolyte is given as

$$\sigma_e^{eff} \nabla \cdot \nabla \phi_e = 0 \tag{6}$$

where, ϕ_e is the local potential in the electrolyte. Electric insulation boundary conditions were applied to all of the channel surfaces. Within the electrodes, where charged species are generated or consumed, a current source is applied and the local current density is calculated by the Butler-Volmer reaction kinetics equation. The potential equation was again used to describe the voltage and current distributions within the solid/porous phase electrodes.

$$\sigma_s^{eff} \nabla \cdot \nabla \phi_s = 0 \tag{7}$$

Effective conductivity of solid and electrolyte phases, in the porous design, are calculated based on the following equations:

$$\begin{aligned} \sigma_s^{eff} &= (1-\varepsilon)^{3/2} \sigma_s \\ \sigma_e^{eff} &= \varepsilon^{3/2} \sigma_e \end{aligned} \tag{8}$$

In this model, the system is assumed to be isothermal, and pressure differences are not large enough to influence diffusion coefficients. Implementing these assumptions allows the concentration distributions of the fuel and oxidant to be described by Fick's law [19] given as

$$\nabla \cdot \left(-D_{eff} \nabla c + c\mathrm{v}\right) = 0 \tag{9}$$

Within the electrode subdomains, a source term is added to the above equation. This results in the following equation:

$$\nabla \cdot \left(-D_{eff} \nabla c + c\mathrm{v}\right) = \frac{e_i}{nF} i_i \tag{10}$$

D_{eff} represents the effective diffusion coefficient which can be calculated directly from the original diffusion coefficient using Eq. (10).

$$D_{eff} = \varepsilon^{3/2} D \tag{11}$$

The Butler-Volmer equation is used to describe the rate of the electrochemical reaction in the cell:

$$i = i_0 \frac{c}{c_{REF}} \left[e^{\left(\frac{\alpha nF}{RT}\eta\right)} - e^{\left(-\frac{(1-\alpha)nF}{RT}\eta\right)} \right] \tag{12}$$

In this equation, η is the activation overpotential. The reactant species are consumed at the consumption rate of S, which is proportional to the current density [13], given as

$$S = \frac{ai}{nF} \tag{13}$$

where a is the specific surface area which is related to the porosity through the equation below:

$$a = \left(\frac{\varepsilon}{\varepsilon_0}\right)^{0.75} A_e \tag{14}$$

in which, ε_0 and A_e are the reference values for the porosity and specific surface area, respectively.

At each electrode, it is necessary to calculate the activation overpotential which is required to overcome irreversibilities as the reaction deviates from its equilibrium state.

$$\eta = \phi_s - \phi_e - E_{REVERSIBLE} \tag{15}$$

RESULTS

Cell polarization curves are used as a quantitative measure for cell performance. In previous studies, the current and power were conventionally normalized by the electrode surface area. However, it is reasonable to normalize the current and power by the overall fuel cell volume, as the output power or current per unit volume is the clearest indication of the fuel cell's effectiveness as a compact power source [11].

Figure 5 compares the polarization curves obtained for microfluidic fuel cells with different cross section aspect ratios (i.e., height to width ratio). The high aspect ratio (presented as High AR in the figures) depicts higher voltage at most current densities. This is due to the higher Peclet number in high aspect ratio geometry and lower ionic resistivity between the anode and cathode (since the anode and cathode are closer to each other compared to the other geometries.). In high aspect ratio, there is a sudden fall at high current densities. This is because that the electrodes are less extended toward the centre of the channel so they can hardly reach out to fresh reactants when it is really required (i.e., high reaction rates). The "Extended Square" configuration is the square cross section with the electrodes extended away from the side walls toward the centre of the channel up to the edges of the mixing region (see Fig. 4. b)). If the electrodes are extended into the mixing region, fuel crossover will occur and reduce the performance of the fuel cell. When the results are presented based on normalizing the current by the surface area, the performance of the cell with the simple square cross section seems to be better than that of the extended square cross section. This misleading result can be explained by the fact that the added surface area by extension does not contribute to the current generation as much as the side wall electrodes do. In other words, normalized by electrode area, the performance of the simple square appears better than the extended square. However, this comparison still leaves some uncertainty as to which is a better design because the larger electrode area of the extended square may compensate for the lower per area output. Normalizing by volume removes this uncertainty and shows conclusively that the greater active area of the extended square does in fact compensate for the lower per area performance and is actually a better design from the point of view of developing a compact power source (see Fig. 6). The fuel utilization of these geometries is also obtained. It is shown that the fuel utilization of the simple square at 0.45V is 13.8% and for the extended square is 15.4%. As for the high and low aspect ratio geometries, it should be mentioned that the main reason for their high power output per unit volume is that there is more electrode surface area incorporated in them (see Fig. 4). The active surface area in low aspect ratio (4.48mm×8mm) is slightly more than what (4.2mm×8mm) is incorporated in high aspect ratio geometry. In spite of the above fact, both geometries have approximately the same power output up to a certain point in the polarization curve. This is because of two reasons: 1) the Peclet number is higher in high aspect ratio; 2) the average ionic resistivity of electrolyte in high aspect ratio compared to the low aspect ratio is lower (since the anode and cathode are closer to each other in high aspect ratio design). These two facts compensate for the slightly smaller active surface area in the high aspect ratio geometry compared to the low aspect ratio one and therefore cause the high aspect ratio design to generate almost the same power output as the low aspect ratio structure. The fuel utilization of both designs is approximately 18% when the cell voltage is 0.45V. The numerical results for the porous electrode design developed in this paper are presented in Fig 7. The results were obtained for two different flow rates (i.e., 60 μlmin^{-1} and 300 μlmin^{-1}). The numerical results presented with solid lines are compared to the experimental data presented by dotted lines. In general, the numerical results follow the same trend as the experimental data. Current densities here are calculated on the basis of the vertically projected area (12mm×1mm) to provide a reasonable comparison with experimental data reported in the literature [11]. The polarization values are also in good agreement with the experimental ones except for the very high current density region (see Fig. 7). The deviation from the experimental values at this region could be justified based on the fact that the exchange current density was assumed to be constant in the model (see the table of constants in Annex B). This is not a very accurate assumption when it comes to high current densities: high current densities require high reaction rates. Since the electrodes are made of carbon, their electric conductivity is not high enough to contribute to a completely even distribution of potential field. As a result, the very beginning of the electrodes, where the wires are attached to, are going to be much more depleted due to the higher reaction rates than the end of the electrodes. This unevenly-distributed potential field leads to different local concentrations, which is the main cause of divergence from the constant exchange current density assumption made in the presented model. However, for the practical cell voltage (i.e., 0.8 V), the exchange current density assumption holds since at this potential, the reaction rates are not that high to be violate this assumption.

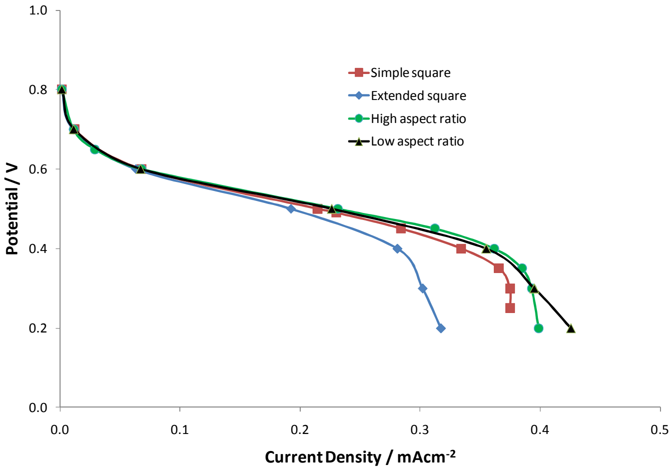

Figure 5 The effect of the channel aspect ratio and electrode geometry (the current is normalized by the surface area)

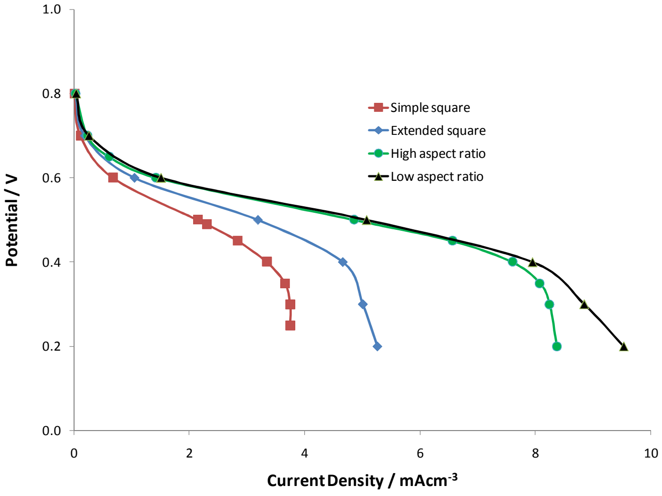

Figure 6 The effect of the channel aspect ratio and electrode geometry (the current is normalized by the cell volume)

Using the above model, the effect of porosity has also been investigated. The results presented in Fig. 8 show that the porosity value around 0.7 is the optimal value. This optimum value depends on different factors including pressure drop across the porous electrode (Δp), the effective diffusion coefficient (D_{eff}), the effective electric conductivity of the electrolyte (σ_e^{eff}) and the electrodes (σ_s^{eff}), and the available surface area (a). The extreme values of porosity clearly show the effect of the above parameters. In essence, low porosity increases the pressure drop across the porous electrode which leads to higher parasitic power loss to drive the electrolyte, and at the same time, it significantly reduces the active surface area which is available in higher porosity values (see Equation 14). Higher porosity, on the other hand, increases the effective diffusion coefficient inside the porous electrode which enhances the species transportation to the active sites. On the negative side, increasing the porosity will decrease the effective electric conductivity of the solid phase which hampers the electrochemical reactions, though it enhances the effective electric conductivity of the electrolyte phase at the same time.

In this work, the effects of all the factors were taken into account to determine the optimum value of the porosity. The results of this work are presented in Fig. 4. They were obtained by keeping the operational parameters (such as the flow rates, cell voltage, cell temperature) as well as the fiber diameter of the porous electrode constant. The results show that a porous electrode with a 67% porosity results in the highest power output.

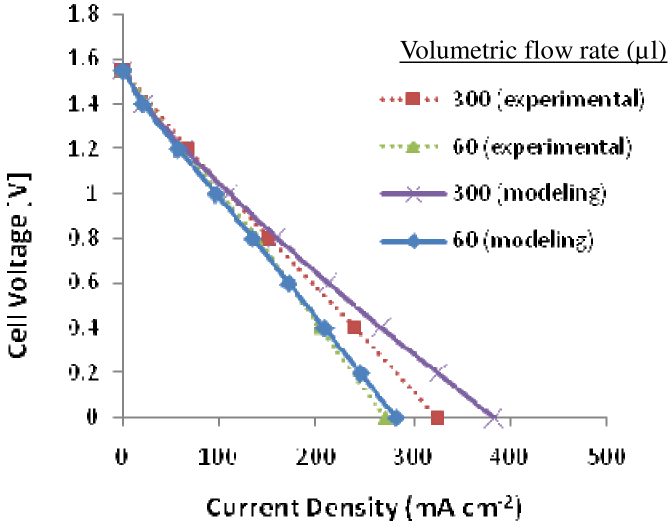

Figure 7 The polarization curves of the microfluidic fuel cell with flow-through porous electrodes. The numerical results are in good agreement with those obtained from experiments [11]

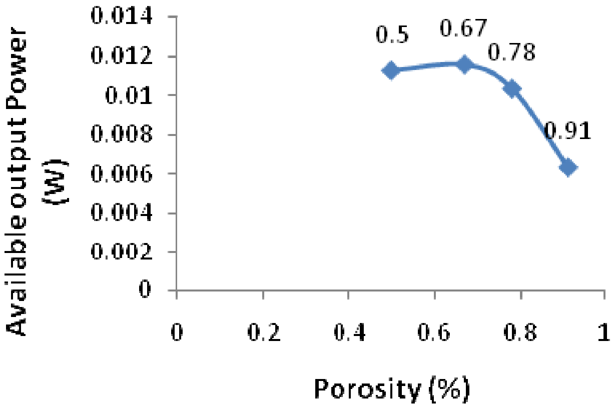

Figure 8 Study the effect of the electrode porosity on the power output of the microfluidic fuel cell

CONCLUSION

In this paper, a comprehensive numerical study has been conducted to compare the performance of the different microfluidic fuel cell designs (e.g., microfluidic fuel cells with different cross section aspect ratios and electrode configurations (non-porous design) and flow-through porous electrode) reported in the literature. Polarization curves were obtained by integrating the normal current density on the cathode boundaries using COMSOL Multiphysics. The fuel utilization of the microfluidic fuel cell with solid (different aspect ratio) and porous electrodes has also been calculated in order to study the effect of the geometrical optimizations and electrode material on the fuel utilization. The fuel utilization of the simple square at 0.45V is 13.8% and for the extended square is 15.4%; however, the fuel utilization of the high and low aspect ratio geometries both is approximately 18% when the cell voltage is 0.45V.

By changing the cross section aspect ratios, it is found that the high and low aspect ratios are better than the square one in performance. At very high current density (i.e., 8 mAcm^{-3} and higher) low aspect ratio is proven to perform better however the high aspect ratio is slightly performing better at lower current densities. It is also shown that the microfluidic fuel cell with the flow-through porous electrode allows for enhanced fuel utilization and high power density at the same time. It is easy to reach to almost 100% fuel utilization with this design (Low flow rate and low cell voltage are required.).

In this study, the effect of the electrode porosity is also investigated and it is demonstrated that the 67% porosity is the optimum value for the electrode porosity in this design.

ACKNOWLEDGMENTS

This work was supported by the Natural Science and Engineering Research Council (NSERC) of Canada.

REFERENCES

[1] A. Bazylak, D. Sinton, N. Djilali, Journal of Power Sources 143 (2005) 57–66.

[2] C.K. Dyer, Journal of Power Sources 106 (2002) 31–34.

[3] G.F. McLean, N. Djilali, M. Whale, T. Niet, Proceedings of the 10th Canadian Hydrogen Conference, 2000, pp. 349–358.

[4] R. Hahn, S. Wagner, A. Schmitz, H. Reichl, J. Power Sources 131 (2004) 73–78.

[5] J. Yu, P. Cheng, Z. Ma and B. Yi, Electrochim. Acta, vol. 48, pp. 1537-1541, 2003.

[6] S. Lee, A. Chang-Chien, S. Cha, R. O'hayre, Y. Park, Y. Saito and F. Prinz, J. Power Sources, vol. 112, pp. 410-418, 2002.

[7] J. Yeom, G. Mozsgai, B. Flachsbart, E. Choban, A. Asthana, M. Shannon and P. Kenis, Sensors & Actuators: B.Chemical, vol. 107, pp. 882-891, 2005.

[8] A. Ozbek, Electronic Design, vol. 51, pp. 102-106, 2003.

[9] M.H. Chang, F. Chen, N.S. Fang, Journal of Power Sources 159 (2006) 810–816.

[10] E. Kjeang, N. Djilali, D. Sinton, Journal of Power Sources 186 (2009) 353–369.

[11] E. Kjeang, R. Michel, D.A. Harrington, N. Djilali, D. Sinton, Journal of the American Chemical Society 130 (2008) 4000–4006.

[12] E. Kjeang, R. Michel, D. Sinton, N. Djilali, D.A. Harrington, Electrochimica Acta
54 (2008) 698–705.

[13] R.S. Jayashree, L. Gancs, E.R. Choban, A. Primak, D. Natarajan, L.J. Markoski, P.J.A. Kenis, Journal of the American Chemical Society 127 (2005) 16758–16759.

[14] R. Ferrigno, A.D. Stroock, T.D. Clark, M. Mayer, G.M. Whitesides, Journal of the American Chemical Society 124 (2002) 12930–12931

[15] R.F. Ismagilov, A.D. Stroock, P.J.A. Kenis, G. Whitesides, Applied Physics Letters 76 (17) (2000) 2376–2378.

[16] A. Li, S.H. Chan, N.T. Nguyen, Journal of Micromechanics and Microengineering 6 (2007) 1107–1113.

[17] S. Motokawa, M. Mohamedi, T. Momma, S. Shoji, T. Osaka, Electrochemistry Communications 6 (2004) 562-565.

[18] J. Yeom, R.S. Jayashree, C. Rastogi, M.A. Shannon, P.J.A. Kenis, Journal of Power Sources, 160 (2006) 1058-1064.

[19] R.B. Bird, W.E. Stewart, E.N. Lightfoot, Transport Phenomena, 2nd ed., John Wiley, New York, 2002.

[20] F. Rahman, M. S. Kazacos, Journal of Power Sources 189 (2009) 1212–1219.

[21] D. You, H. Zhang, J. Chen, Electrochimica Acta 54 (2009) 6827–6836.

[22] T. Yamamura, N. Watanabe, T. Yano, Y. Shiokawa, Journal of The Electrochemical Society, 152 (4) A830-A836 (2005).

ANNEX A

SOME OF THE CONSTANTS USED IN THE ANODIC AND CATHODIC FLOWS (SOLID ELECTRODE DESIGN)

Parameter	Anode	Cathode
Density, ρ^*	1000 kgm^{-3}	
Dynamic viscosity, μ^*	0.001 Pas	
Faraday constant, F	96485.34 Cmol^{-1}	
Cell temperature, T	298 K	
Universal gas constant, R	8.314 Jmol^{-1}K^{-1}	
Ionic conductivity, σ^*	11.47 Sm^{-1}	43 Sm^{-1}
Diffusion coefficient, D^{**}	8.3e-10 m^{2}s^{-1}	8.3e-10m^{2}s^{-1}
Charge transfer coefficient, α^*	0.5	0.5
Number of electrons transferred, n^*	2	4
Exchange current density, i_0^*	3.82e5 Am^{-3}	100 Am^{-3}
Inlet concentration, c_0^*	2100 molm^{-3}	0.5 molm^{-3}

* The value is obtained from [9].
** An approximated value for the diffusion of relatively small molecules in an aqueous solution is assumed [1].

ANNEX B

SOME OF THE CONSTANTS USED IN THE ANODIC AND CATHODIC FLOWS (POROUS ELECTRODE DESIGN)

Parameter	Anode	Cathode
Density, ρ^*	1410 kgm^{-3}	
Dynamic viscosity, μ^*	5.67e-3 Pas	
Faraday constant, F	96485.34 Cmol^{-1}	
Cell temperature, T	298 K	
Universal gas constant, R	8.314 J/(Jmol^{-1}K^{-1})	
Ionic conductivity, σ^*	59 Sm^{-1}	59 Sm^{-1}
Ref. Concentration, c_{REF}	1000 molm^{-3}	1000 molm^{-3}
Diffusion coefficient, D^{****}	9.78e-9 m^{2}s^{-1}	9.78-9m^{2}s^{-1}
Charge transfer coefficient, α^{**}	0.5	0.5
Number of electrons transferred, n	1	1
Exchange current density, i_0	19.7 Am^{-3}	139 Am^{-3}
Reversible potential, $E_{REVERSIBLE}$	-0.496 V	0.750 V
Inlet concentration, c_0^{***}	2000 molm^{-3}	2000 molm^{-3}
Reference porosity, ε_0^{**}	0.929	
Reference specific surface area, A_e^{**}	1.62e4 m^2	

* The value is obtained from [20].
** The value is obtained from [21].
*** The value is obtained from [11].
**** An estimated value is assumed from [22] to fit to the experimental results from [11].